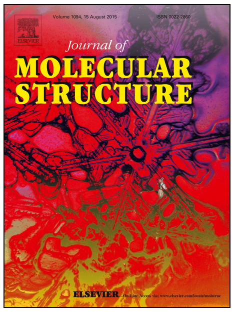

Crystallographic elucidations of indium(III) porphyrin conformations, morphology and aggregation behaviour: Comparative optical study of free base porphyrins and their indium(III) derivatives at varying pH

Padma Dechan, Gauri Devi Bajju, Puneet Sood, Umar Ali Dar

PII: S0022-2860(19)30075-4

DOI: https://doi.org/10.1016/j.molstruc.2019.01.064

Reference: MOLSTR 26115

To appear in: *Journal of Molecular Structure*

Received Date: 4 October 2018

Revised Date: 18 January 2019

Accepted Date: 18 January 2019

Please cite this article as: P. Dechan, G.D. Bajju, P. Sood, U.A. Dar, Crystallographic elucidations of indium(III) porphyrin conformations, morphology and aggregation behaviour: Comparative optical study of free base porphyrins and their indium(III) derivatives at varying pH, *Journal of Molecular Structure* (2019), doi: https://doi.org/10.1016/j.molstruc.2019.01.064.

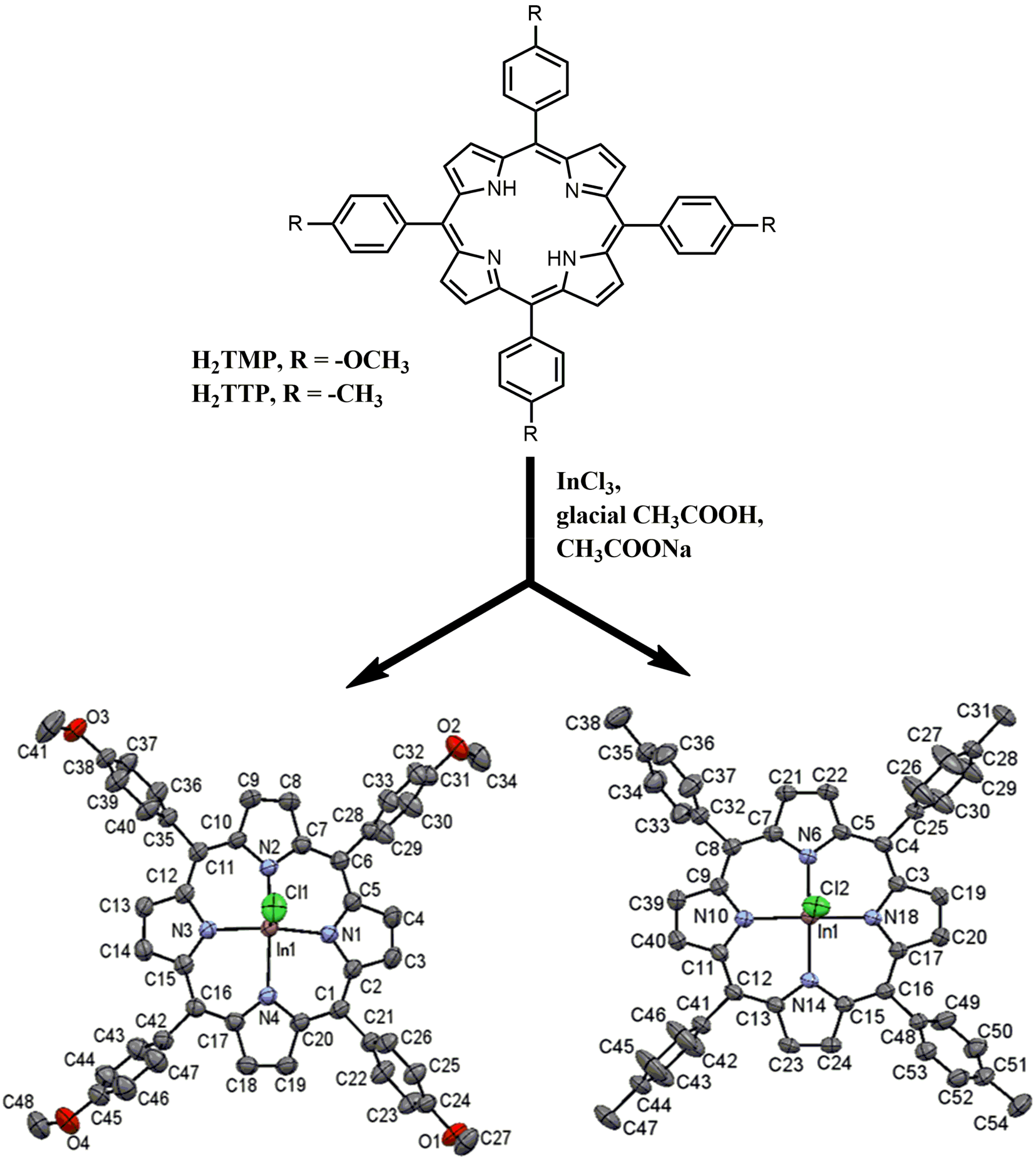

[In(III)(TMP)]Cl

[In(III)(TTP)]Cl

Crystallographic elucidations of indium(III) porphyrin conformations, morphology and aggregation behaviour: Comparative optical study of free base porphyrins and their indium(III) derivatives at varying pH

Padma Dechan[a], Gauri Devi Bajju[a*], Puneet Sood[b] and Umar Ali Dar[a]

[a]Postgraduate Department of Chemistry, University of Jammu, Jammu-180006, India

[b]Advanced Materials Research Centre, Block- A2, Kamand Campus, Indian Institute of Technology, Mandi, Himachal Pradesh, 175005, India

Abstract

The supramolecular structural architectures of 5, 10, 15, 20-Tetrakis-(4-methoxyphenylporphyrinato) indium(III) chloride (**I**) and 5, 10, 15, 20-Tetrakis-(4-methylphenylporphyrinato) indium(III) chloride (**II**) have been determined from their three dimensional X-ray diffraction data. Complex **I** crystallizes in the orthorhombic space group, Pbca with a = 23.0083(4) Å, b = 15.2447(3) Å, c = 23.3737(4) Å, $\alpha = \beta = \gamma = 90°$, V = 8198.5(3) Å^3 and Z = 8, whereas complex **II** crystallizes in the triclinic space group, P-1 with a = 12.0737(5) Å, b =12.1000(5) Å, c =14.1682(6) Å, α = 88.560(3)°, β = 78.730(3)°, γ = 78.280(3)° V = 1987.40(14) Å^3 and Z = 2. The geometries around In^{+3} ions in both the complexes are square pyramidal giving dome shaped architectures to the metalloporphyrins. In their respective crystal lattices, the monomeric units of complex **I** and **II** are packed in J-type (head-to-tail) supramolecular aggregation. These monomers are linked into their three dimensional supramolecular networks by various non covalent forces. Further the packing of monomers of each complex in their respective unit cells leaves significant void volumes (porosities). The optical absorption spectra of complex **I** and **II** and their free base analogs i.e. 5, 10, 15, 20-Tetrakis-(4-methoxyphenyl) porphyrin, **H$_2$TMP** and 5, 10, 15, 20-Tetrakis-(4-methylphenyl) porphyrin, **H$_2$TTP** have also been investigated in CH_2Cl_2 at different ionic strengths of the media. The investigations revealed that both the free bases exist as simple monomers, j-aggregates and dianionic monomers at neutral (pH = 7), acidic (pH = 4 and lower) and basic (pH = 10) media conditions. Also at high ionic strength of the media, the free bases undergo charge transfer electronic transitions. The two In^{3+} porphyrin exists as simple monomers at pH = 7. However at pH = 5 and lower, the In^{3+} ions in complex **II** is remarkably easily replaced by the protons of the acid to generate the corresponding protonated free base monomers which simultaneously aggregate in J-type stacking mode. In contrast to complex **II** that exhibits low stability in acidic media, the complex **I** remain intact in such media reflecting extremely high stability of the complex. The insertion of In^{3+} ions into the porphyrinic cores of free bases causes bathochromic shift followed by increase in the intensities of absorption bands. The appearance of two set of doublets for ortho phenyl protons in the ^{1}H NMR spectra of each complex is attributed to the magnetic inequivalence of their ortho phenyl protons caused by the pulling of In^{+3} ions above the mean porphyrin planes.

Keywords: dome shaped, mean porphyrin planes, J-type stacking, absorption bands, charge transfer electronic transitions, magnetic inequivalence

Corresponding author: Gauri Devi Bajju*
E-mail: gauribajju@gmail.com
Contact No.: +91 9419145184

1. Introduction

Porphyrin photosensitizers are widely used in numerous applications such as photodyanamic therapy (PDT) [1], solar energy harvesting [2, 3], artificial photosynthesis [4], photodynamic destruction of viruses [5], magnetic resonance imaging (MRI) for the detection of cancer cells [6] etc. For e.g. 5, 10, 15, 20-Tetraphenylporphyrinato indium(III) chloride, **TPPInCl** is an efficient photosensitizer in the photooxidation of L-tryptophan (Trp) and bovine serum albumin (BSA) [7]. The In^{3+} ion in **TPPInCl** induces spin-orbit coupling (heavy atom effect) favouring long lifetime of the triplet excited state in order to efficiently generate singlet molecular oxygen [7]. The high photosensitizing ability of **TPPInCl** suggests that indium porphyrins can serve as potential photosensitizers in photodyanamic therapy and other photo responsive devices such as organic light-emitting diodes and organic thin-film transistors. In order to understand the potential behaviour of π conjugated porphyrins in various biological and material applications, characterisation of macro rings as an individual molecule and their crystal packing modes are essential. The first indium derivatives of metalloporphyrins i.e. **TPPInCl**, **TTPInCl** and **TMPInCl** were reported by Bhatti et al [8]. These metalloporphyrins were characterised by ^{1}H NMR spectroscopy, Uv-Vis spectroscopy and elemental analysis. Later, the first single crystal of an indium porphyrin, 5, 10, 15, 20-tetrakis-(phenylporphyrinato) indium(III) chloride, **TPPInCl** was reported in 1980 [9]. Eventually many more single crystals of In^{3+} porphyrins were reported in the literature [10-14]. In all the reported structures, the In^{3+} ion is displaced from the core planes due to its higher ionic radius (0.8 Å). The magnitude of displacement of the metal ion from the core porphyrinic plane seems to be controlled by various peripheral substitutions around the porphyrin ring and axial substitutions on the metal centre. Though, the two In^{3+} complexes i.e. **TMPInCl** and **TTPInCl** were successfully synthesized by Bhatti et al [8], the single crystals of these complexes have not been reported in the literature and in fact the complexes seems not to have given adequate attention. As a result many interesting chemistry of **TMPInCl** and **TTPInCl** are yet to be explored. In an attempt to grow the single crystals of **TMPInCl** and **TTPInCl**, we reiterated the synthesis of **TMPInCl** and **TTPInCl** following the method described by Bhatti et al [8]. After many attempts, we were finally successful in getting fine needle shaped and violet colored crystals of **TMPInCl** and **TTPInCl**. The complexes crystallized in the orthorhombic and triclinic unit cells. Each complex have highly ruffled structures with In^{3+} ion being displaced out of the N4 core planes, giving “dome shaped” architectures to the metalloporphyrins. The effect of pH on the electronic absorption spectra of the free base analogues of **I** and **II** i.e. **H_2TMP** and **H_2TTP** have also been investigated in non aqueous media and the results have been discussed in detailed. Porphyrins are known to undergo dramatic self aggregation under certain conditions [15-17]. Porphyrins aggregate either in J-type (head-to-tail) fashion or H-type (face-to-face) fashion [18]. The J-type stacking involves prominent red shift of monomeric absorption bands, in particular the B band [19, 20] and the H-type stacking involves blue shift of monomeric absorption bands [21, 22]. The J-type molecular alignments have been observed in the three dimensional crystal lattice of the each synthesized complex and in the aggregated states of **H_2TMP** and **H_2TTP**. The schematic diagram 1 shows the structures of the two free base porphyrins, under neutral (a), acidic (b) and basic media conditions (c). The structures of In^{3+} porphyrins, **I** and **II** are also given in scheme 1 (d).

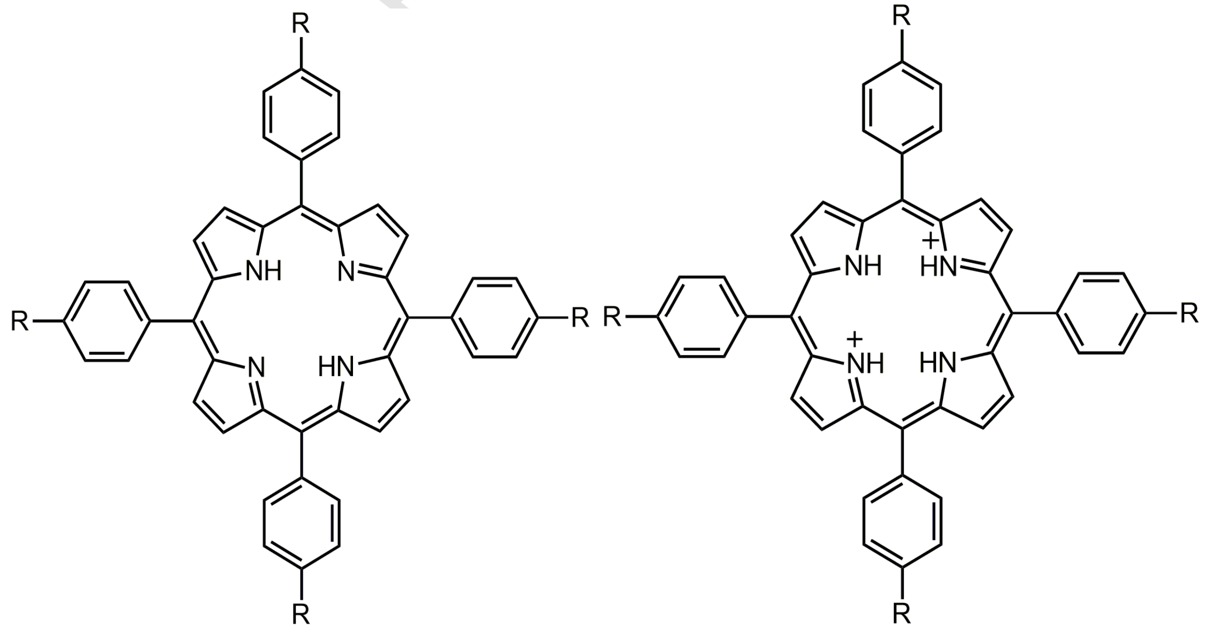

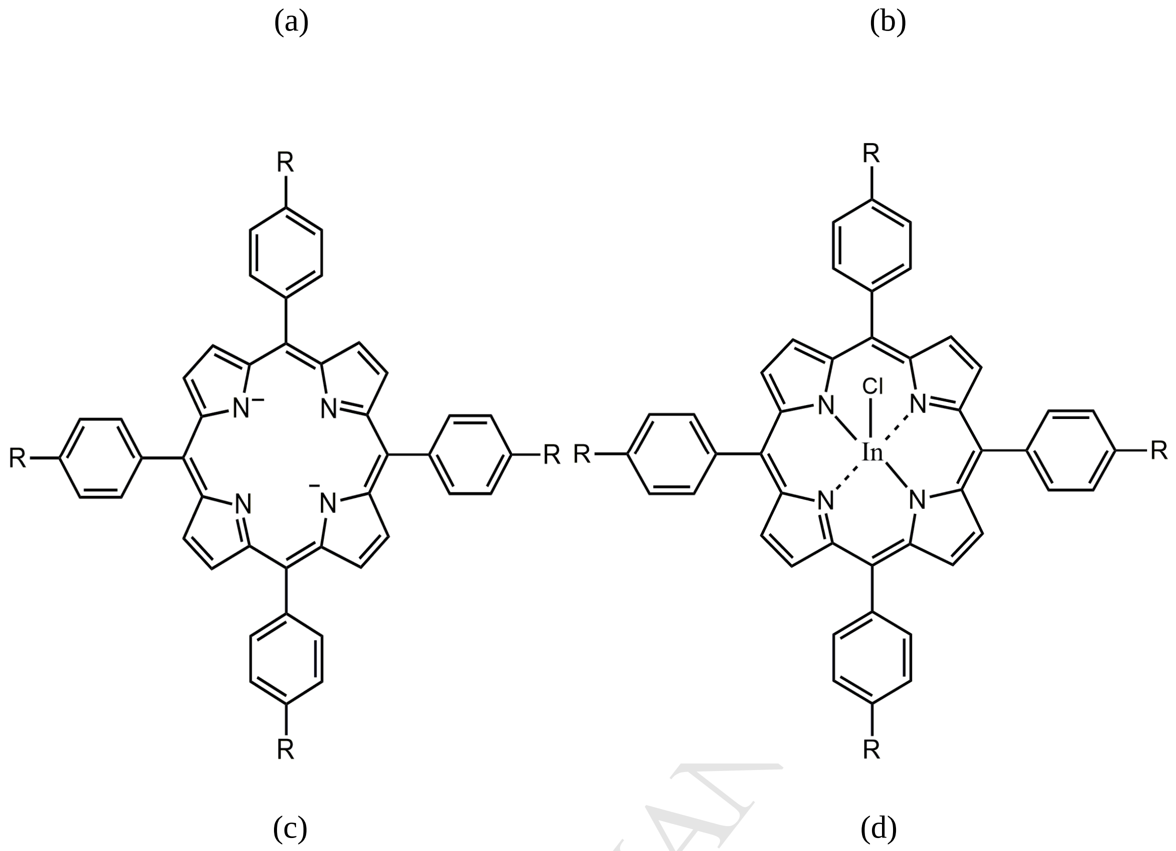

R = $-OCH_3$, $-CH_3$

Scheme 1 Structures of **H_2TMP** and **H_2TTP** at (a) pH = 7 (b) pH = 4 and lower (c) pH = 10 (d) structures of **I** and **II**

2. Experimental

2.1 Materials and reagents

The analytical grades chemicals were used for the synthesis of the starting materials i.e. **H_2TMP** and **H_2TTP** and their In^{3+} derivatives i.e. **I** and **II**. Pyrrole, 4-methoxybenzaldehyde, 4-methylbenzaldehyde, propionic acid, diethylether, glacial acetic acid, sodium acetate, methanol, dichloromethane, chloroform, basic alumina and silica gel were purchased from sigma Aldrich as were used as received. $InCl_3$ was also purchased from sigma Aldrich.

2.2 Measurements and Instrumentation

UV-Visible spectra were obtained on PG spectrophotometer; model T-90. ^{1}H NMR spectra were recorded on Bruker spectrometer, model AV 400 N (400 MHZ), using $CDCl_3$ as solvent and TMS as internal reference. FT-IR spectra were recorded between 4000 cm^{-1} to 400 cm^{-1} using KBr pellets on Perkin Elmer Spectrum.

2.3 Solution and Refinement of the Crystal Structures of **I** and **II**

Reflection data were measured at 293(2) K. The crystal was mounted under paratone oil and to get relative intensity data, the single crystal analysis was collected on a CCD Agilent SUPERNOVA E (Dual) diffractometer using monochromated Cu-Kα radiation (λ = 0.154184 Å) at 293(2) K. Using Olex2 [23], the structure was solved with the ShelXS [24] structure solution program using Direct Methods and refined with the ShelXL [24] refinement package using Least Squares minimisation. The positions of all the atoms were obtained by direct method. All non hydrogen atoms were refined anisotropically. The remaining H- atoms were refined with isotropic temperature factors, 1.2 U_{eq} of their parent atoms. Crystallographic data (cif) has been deposited with the Cambridge Structural Data Centre with reference numbers- 1584380 and 1584382.

2.4 Synthesis of **H_2TMP** and **H_2TTP**

The two starting compounds i.e. **H_2TMP** and **H_2TTP** were synthesized according to the modified Adler's method [25]. Pyrrole (20mmols) and para-substituted benzaldehydes (20mmols) were added to the propionic acid solutions (50ml) in a 250ml round bottomed flasks fitted with water condensers. The reaction mixtures were then allowed to reflux for half an hour at 60˚C, as shown in scheme 2. After the completion of the reaction, the reaction mixtures were allowed to cool at room temperature and then stored in refrigerator for 2 hours. The shiny purple crude products of **H_2TMP** and **H_2TTP** were then filtered and the residues were air dried completely. The crude products were then subjected to their purifications on basic alumina columns using methanol in case of **H_2TMP** and chloroform in case of **H_2TTP** as eluting solvents. The purified compounds were finally recovered by the evaporation of the organic solvents.

H_2TMP was obtained as purple solid with 60% yield. FT-IR (KBr, ν_{max}, cm^{-1}): 3317.66 ν(N-H)pyrrole, 730.46 γ(C-H)ph, 800.04 γ(C-H)pyrrole, 1341.22 ν(C-N), 1595.22 ν(C=N), 2913.18 ν(C-H) OCH_3, 1023.84 $\nu(C\text{-}O\text{-}C)_{sym}$, 1233.98 $\nu(C\text{-}O\text{-}C)_{asym}$. ^{1}H NMR (CDCl3, 400MHz, δ, ppm): -2.74 (s., 2H, NH), 4.12 (s., 12H, OCH_3), 7.31-7.33 (d., 8H, ArH_m), 8.14-8.16 (d., 8H, ArH_o), 8.89 (s., 8H, βH). UV-Vis (λ_{max}, nm, CH_2Cl_2): 421 (B band), 519, 555, 594, 651 (Q bands).

H_2TTP was obtained as purple solid with 70% yield. FT-IR (KBr, ν_{max}, cm^{-1}): 3327.35 ν(N-H)pyrrole, 735.87 γ(C-H)ph, 800.49 γ(C-H)pyrrole, 1352.16 ν(C-N), 1583.63 ν(C=N), 2912.64 ν(C-H) OCH_3, 1022.32 ν(C-O-C)$_{sym}$, 1221.96 ν(C-O-C)$_{asym}$. ^{1}H NMR (CDCl3, 400MHz, δ, ppm): -2.74 (s., 2H, NH), 2.73 (s., 12H, CH_3), 7.57-7.59 (d., 8H, ArH$_m$), 8.11-8.13 (d., 8H, ArH$_o$), 8.88 (s., 8H, βH). UV-Vis (λ_{max}, nm, CH_2Cl_2): 420 (B band), 516, 552, 592, 644 (Q bands).

2.5 Synthesis of **I** and **II**

The In^{3+} derivatives of **H_2TMP** and **H_2TTP** i.e. **I** and **II** were synthesized by acetate method according to the procedure described by Bhatti et al [8]. 246 mg (0.4 mmols) of the starting compounds and 221 mg (1.0mmols) of the metal carriers i.e. $InCl_3$ were added in 250 ml round bottomed flasks fitted with water condensers and loaded with glacial acetic acids (30 ml) and sodium acetates (0.554 g). The reaction mixtures were then refluxed for 4 hours at 60˚C. The progresses of the reactions were determined spectrophotometrically. After the completion of the reaction, the reaction mixtures were allowed to cool at room temperature and then brought to 0˚C by placing the mixtures on ice baths. This method induces rapid crystallisation of the products so formed. The crude products of **I** and **II** were purified on silica gel columns using dichloromethane as an eluent. The metal complexes were further re-crystallized from mixed solvent systems of dichloromethane and Hexane (2:1). The needle shaped single crystals of the metal complexes, **I** and **II** were obtained by slow evaporation of the chloroform solutions.

[In(III)TMP]Cl [I] was obtained as violet solid with 40% yield. FT-IR (KBr, ν_{max}, cm^{-1}): 720.44 γ(C-H)ph, 806.28 γ(C-H)pyrrole, 1339.62 ν(C-N), 1572.05 ν(C=N), 2932.89 ν(C-H) OCH_3, 1064.75 ν(C-O-C)$_{sym}$, 1247.03 ν(C-O-C)$_{asym}$. ^{1}H NMR (CDCl3, 400MHz, δ, ppm): 4.14 (s., 12H, OCH_3), 7.36-7.38 (d., 8H, ArH$_m$), 8.04-8.06 (d., 8H, ArH$_o$), 8.30-8.32 (d., 8H, ArH$_o$), 9.12 (s., 8H, βH). UV-Vis (λ_{max}, nm, CH_2Cl_2): 430 (B band), 563, 606 (Q bands).

[In(III)TTP]Cl [II] was obtained as violet solid with 35% yield. FT-IR (KBr, ν_{max}, cm^{-1}): 723.34 γ(C-H)ph, 800.49 γ(C-H)pyrrole, 1336.73 ν(C-N), 1573.98 ν(C=N), 2923.25 ν(C-H) OCH_3, 1069.57 ν(C-O-C)$_{sym}$, 1251.86 ν(C-O-C)$_{asym}$. ^{1}H NMR (CDCl3, 400MHz, δ, ppm): 2.75 (s., 12H, CH_3), 7.63-7.65 (d., 8H, ArH$_m$), 8.01-8.03 (d., 8H, ArH$_o$), 8.27-8.29 (d., 8H, ArH$_o$), 9.10 (s., 8H, βH). UV-Vis (λ_{max}, nm, CH_2Cl_2): 426 (B band), 560, 601 (Q bands).

3. Results and Discussion

The two free base porphyrins and their corresponding In^{3+} derivatives were synthesized according to the methods provided in the literature [25, 8] (scheme 2).

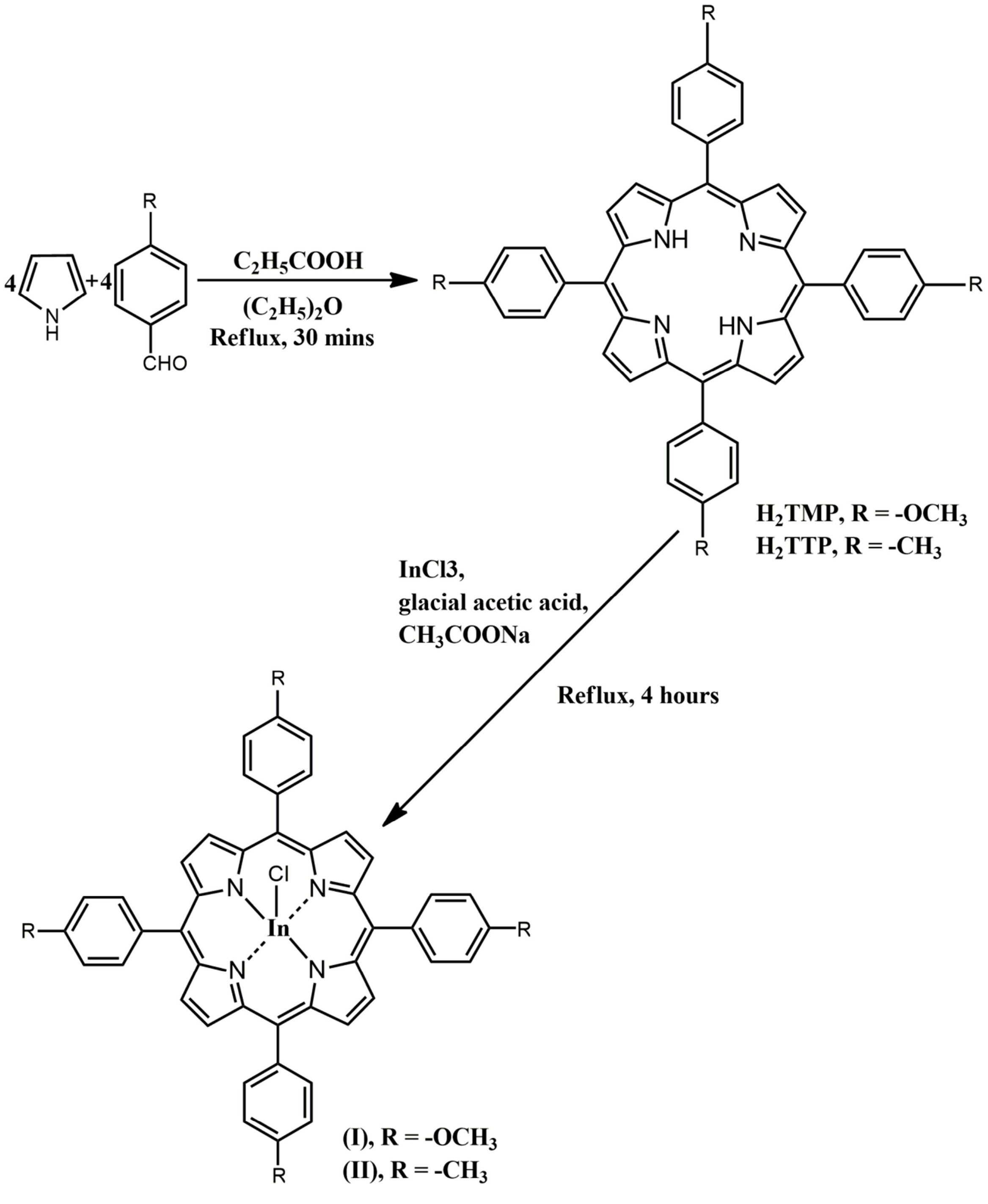

Scheme 2 Synthetic routes for **H$_2$TMP**, **H$_2$TTP** and their In^{3+} complexes, **I** and **II**

3.2 Crystal structures

I and **II** crystallizes in the orthorhombic and triclinic unit cells. The Ortep representations of **I** and **II** along with their crystallographic labelling schemes are given in Fig. 1. The asymmetric unit in each complex consists of single porphyrin molecule. The geometries around the In^{3+} ions in both the metalloporphyrins are regular square pyramidal type, with N(1)/N(2)/N(3)/N(4) and N(6)/N(10)/N(14)/N(18) lying in the basal planes. The 24 atoms porphyrin cores in **I** and **II** are nearly planar [dihedral angle~5.07° (**I**) and~5.03° (**II**)]. In each complex, the In^{3+} ion due to its large ionic radius (0.8 Å) is pulled upward towards the axial chlorine atom and above the mean N4 core plane as shown in Fig. 2. Such phenomenon is known as "doming" of the macrocyclic rings. The average In−N bond distances are 2.146 Å (**I**) and 2.153 Å (**II).** This measured bond distances in **I** and **II** are smaller than that observe in case of **TPPInCl**. The average In−N bond distance in **TPPInCl** was found to be 2.156 (6) Å [9]. Similarly the average N−N distances are 2.916 Å (**I**) and 2.931 (**II**). The larger In−N and N−N bond distances in **II** compared with that of **I** might be attributed to greater expansion of the porphyrin core in **II** than **I**. The In−Cl bond distances are 2.381 Å in both the metal complexes which is slightly larger than that observe in case of **TPPInCl** i.e. the In−Cl bond distance in **TPPInCl** was found to be 2.369 (2) Å [9]. The four phenyl rings in each complex are twisted by~45° with respect to the mean N4 core plane showing significant out of plane distortions. The dihedral angles between the mean plane of 4N and the planes of the phenyl groups are 44.94° [C(24)], 45.57° [C(31)], 45.38° [C(38)] and 45.05° [C(45)] in (**I**) and 44.51° [C(51)], 44.85° [C(44)], 44.47° [C(35)] and 45.86° [C(28)] in (**II**). The greater out of mean plane distortion of the peripheral p-substituted phenyl rings in each metal complex might be attributed to two factors i.e. distortion of In^{3+} ion above the mean N4 plane and steric interactions between the neighbouring phenyl protons and beta pyrrole protons [H29···H8 3.673 Å, H33···H4 3.589 Å, H36···H9 2.560 Å, H26···H3 3.440 Å, H22···H19 3.012 Å, H47···H18 2.843 Å, H43···H14 2.813 Å , H40···H13 2.923 Å] (**I**) and [H30···H22 3.593 Å, H37···H21 2.968 Å, H33···H39 3.014 Å, H40···H42 3.851 Å, H46···H23 3.689 Å, H53···H24 2.497 Å, H49···H20 2.682 Å, H19···H26 3.886 Å] (**II**) (Fig. 3). The phenyl rings in both **I** and **II** are twisted to a lesser extends than that observe in case of **InTPPCl** [9].

The porphyrin monomers in **I** are packed in an offset-stacked geometrical fashion. Such type of stacking is typical of J-type stacking exhibited by certain dye molecules [26-28]. In general a face centred stacking is preferred when electron-rich aromatics (donors) interact with electron-deficient aromatics (acceptors) [29]. Such interactions can be better described as ''aromatic donor–acceptor interactions'' [30]. In the offset packing modes of **I**, the eight porphyrin monomers of the orthorhombic unit cell acts remarkably as four set of offset porphyrin pairs (Fig. 4). The two offset porphyrin pairs lying towards the centre of the unit cell are shown by blue and green colours, where as the other two offset porphyrin pairs lying partly inside and partly outside the orthorhombic unit cell are shown as pink for clarity (Fig. 5). The two offset porphyrin pairs (blue and green) are interlinked by four types of close non covalent intermolecular forces of which C···C, C−H··π, In−Cl···H and C−O···H interactions are present (Fig. 6 and Fig. 7). The closest C···C, In−Cl···H and C−O···H distances are found to be 3.433, 3.249 and 2.527 Å. The In−Cl···Hand C−O···H intermolecular hydrogen bonding interactions are induced by Cl atoms attached axially to the metal centres and the O atoms of para methoxy substituents of four peripheral phenyl rings. The monomeric subunits of each of the two porphyrin pairs (blue and green) are bound to each other by C···C, C−H··π and C−O···H interactions. The absence of In−Cl···Hinteractions in this case is attributed to the non directional orientations of In−Cl and C−H bonds of the interlinked monomers. Though the monomeric subunits of each of the two offset porphyrin pairs (shown as pink) due to their greater centroid to centroid distance (11.83 Å) exhibits no inter porphyrin molecular interactions. However, they are able to interact with their neighbouring porphyrin moieties belonging to other two offset porphyrin pairs (blue and green) by all the four non covalent forces discussed earlier. The hydrogen bonds in **I** are listed in Table 2. The 3D crystal packing in **II** is relatively simpler as compared to 3D packing in **I**. In the triclinic unit cell of **II**, the two porphyrin macrocyles are stacked in an offset (J-type) supramolecular fashion similar to **I**. The two macrocycles are held together by C···C and C−H··π interactions with closest atom to atom of distances (C···C 3.661 Å) as shown in Fig. 8. The centroid to centroid and vertical distances between the porphyrin monomers are 6.36 Å and 4.23 Å. In their respective three dimensional crystal lattices, the “dome-shaped" macrocycles in each complex are packed in such a manner, so that the top of “domes” of the non covalently interlinked porphyrin subunits are facing outwards, thereby leaving many empty spaces in their respective crystals. As a result, clear porosities can be observed in the packing diagrams of **I** and **II** (Fig. 9).

Table 1 Numerical details of the solution and refinement of **I** and **II**

	I	**II**
Empirical formula	$C_{48}H_{36}ClInN_4O_4$	$C_{48}H_{36}ClInN_4$
Formula weight	883.08	819.08
Temperature/K	293(2)	293(2)
Crystal system	orthorhombic	triclinic
Space group	Pbca	P-1
a/Å	23.0083(4)	12.0737(5)
b/Å	15.2447(3)	12.1000(5)
c/Å	23.3737(4)	14.1682(6)
α/°	90.00	88.560(3)

β/°	90.00	78.730(3)
γ/°	90.00	78.280(3)
Volume/Å^3	8198.5(3)	1987.40(14)
Z	8	2
ρ_{calc}g/cm^3	1.431	1.369
μ/mm^{-1}	5.610	5.663
F(000)	3600.0	836.0
Crystal size/mm^3	0.407 × 0.117 × 0.098	0.106 × 0.09 × 0.085
2Θ range for data collection/°	7.68 to 133.74	7.62 to 133.86
Index ranges	$-19 \le h \le 27$, $-18 \le k \le 8$, $-27 \le l \le 26$	$-14 \le h \le 11$, $-12 \le k \le 14$, $-16 \le l \le 16$
Reflections collected	16444	12513
Independent reflections	7211 [R_{int} = 0.0308, R_{sigma} = 0.0385]	6972 [R_{int} = 0.0260, R_{sigma} = 0.0379]
Goodness-of-fit on F^2	1.085	1.038
Final R indexes [I>=2σ (I)]	R_1 = 0.0383, wR_2 = 0.1047	R_1 = 0.0289, wR_2 = 0.0739
Final R indexes [all data]	R_1 = 0.0484, wR_2 = 0.1122	R_1 = 0.0333, wR_2 = 0.0771
Largest diff. peak/hole / e Å^{-3}	0.78/-1.14	0.50/-0.44

Table 2 Hydrogen bonds for **I**

D—H···A	d(D-H)	d(H···A)	d(D···A)	<(DHA)
C27—H27B···Cl1	0.960	3.301	4.076	139.15
C25—H25···Cl1	0.930	3.389	4.306	169.37
C34—H34C···Cl1	0.960	3.011	3.711	130.84
C30—H30···Cl1	0.930	2.913	3.842	178.33
C41—H41A···Cl1	0.960	3.363	3.942	120.81
C48—H48C···Cl1	0.960	3.249	3.988	135.22
C34—H34C···O4	0.960	2.726	3.411(7)	128.83
C48—H48B···O2	0.960	2.779	3.452(7)	127.85
C14—H14···O2	0.930	2.486	3.216(4)	135.49
C13—H13···O2	0.930	3.395	3.597	101.45
C29—H29···O3	0.930	2.527	3.436(5)	165.74

Symmetry code: x, y, z

Table 3 Selected bond lengths (Å) and bond angles (˚) in **I** and **II**

	I		**II**		**I**		**II**
C11-C35	1.485(4)	C17-C16	1.416(4)	C17-C16 C15	125.7(3)	C11-C12-C13	126.0(2)
C16-C42	1.506 (5)	C9-C8	1.405(4)	C2-C1-C20	125.5(3)	C7-C8-C9	125.8(2)
C21-C1	1.501(5)	C12-C41	1.509(3)	C2-C1-C20	125.5(3)	C15-C16-C17	125.6(2)
O3-C38	1.361(4)	C5-C4	1.407(4)	C38-O3-C41	118.2(3)	C3-C4-C5	125.8(2)
O4-C45	1.369(5)	C51-C54	1.516(4)	C31-O2-C34	117.6(3)		
C20-C1	1.409(5)	C3-C4	1.401(4)	C24-O1-C27	117.2(3)		
O2-C31	1.364(4)	C8-C32	1.500(4)	C45-O4-C48	117.0(5)		
C28-C6	1.493(5)	C8-C7	1.405(4)	C12-C11-C10	125.6(3)		
O1-C24	1.366(4)	C11-C12	1.399(4)	C7-C6-C5	126.0(3)		
C12-C11	1.404(5)	C28-C31	1.518(4)				
C7-C6	1.396(5)	C16-C48	1.499(3)				
C10-C11	1.409(5)	C16-C15	1.398(4)				
C15-C16	1.415(5)	C13-C12	1.408(4)				
C1-C2	1.401(5)	C35-C38	1.510(5)				

C5-C6	1.406(5)	C25-C4	1.498(3)
C17-C16	1.397(5)	C44-C43	1.333(7)

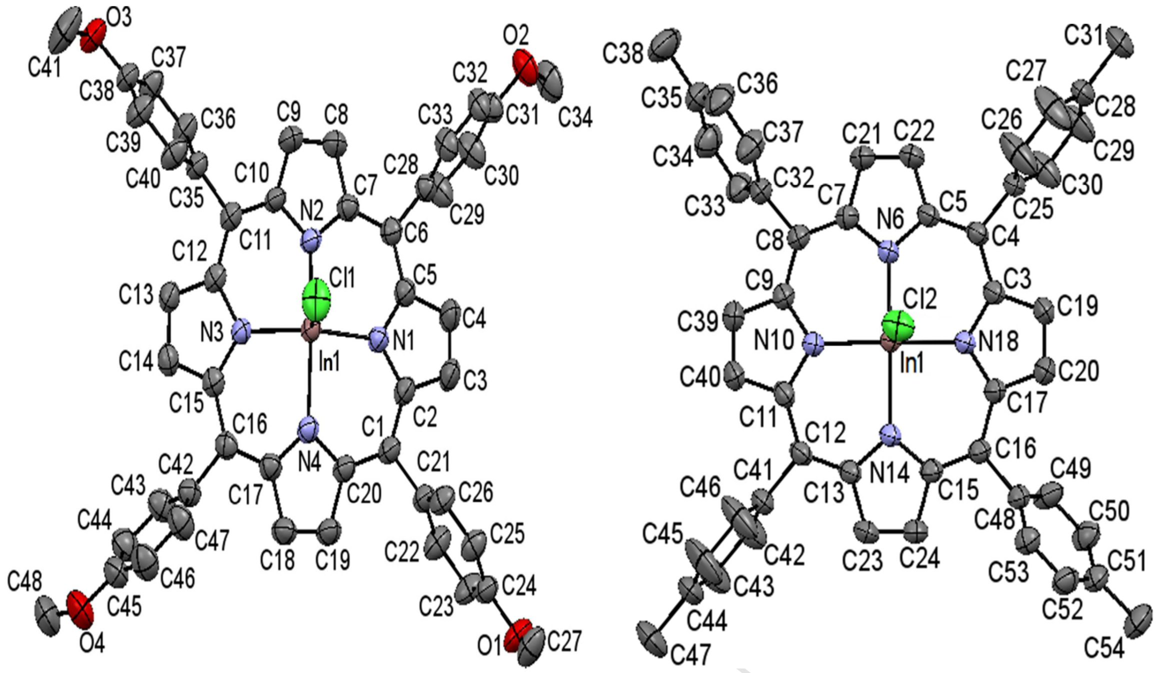

Fig. 1 ORTEP representations of the molecular structures with atom-labeling schemes for **I** (left) and **II** (right). Ellipsoids are shown at 50% probability level. Hydrogen atoms are omitted for clarity

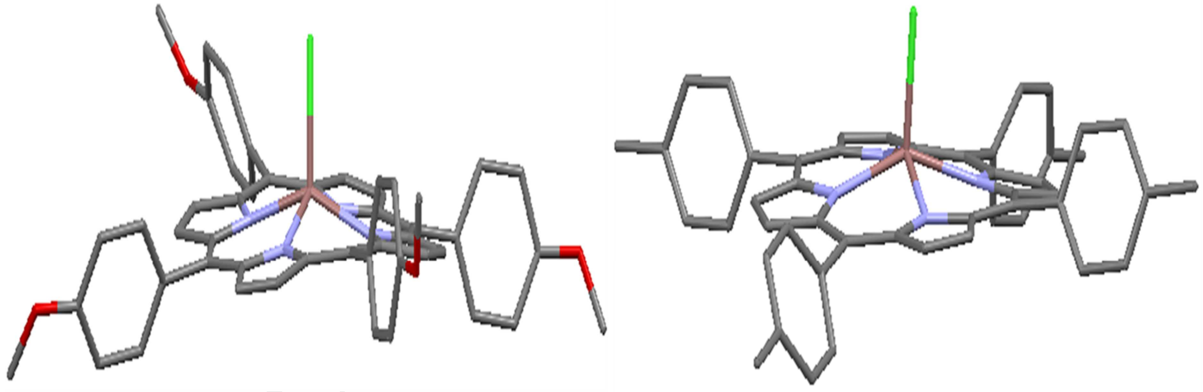

Fig. 2 Ortep views of **I** (left) and **II** (right) illustrating the pulling of indium atoms above the N4 core planes. Hydrogen atoms are omitted for clarity

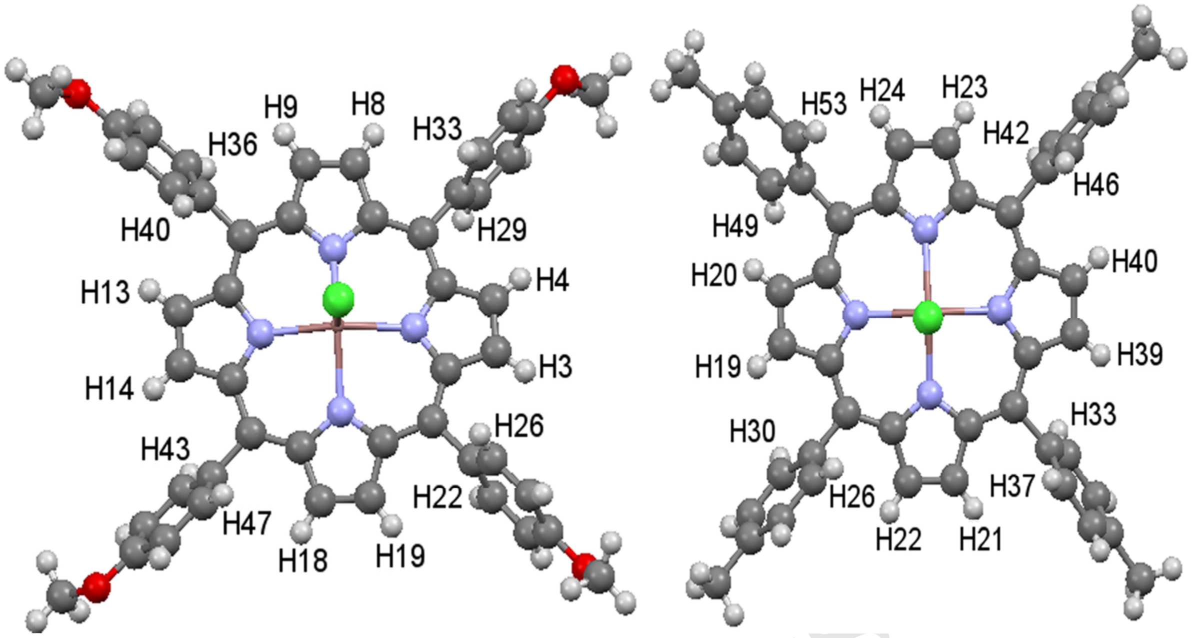

Fig. 3 Steric interactions between the neighbouring phenyl protons and beta pyrrole protons of **I** (left) and **II** (right) causing the twisting of phenyl rings

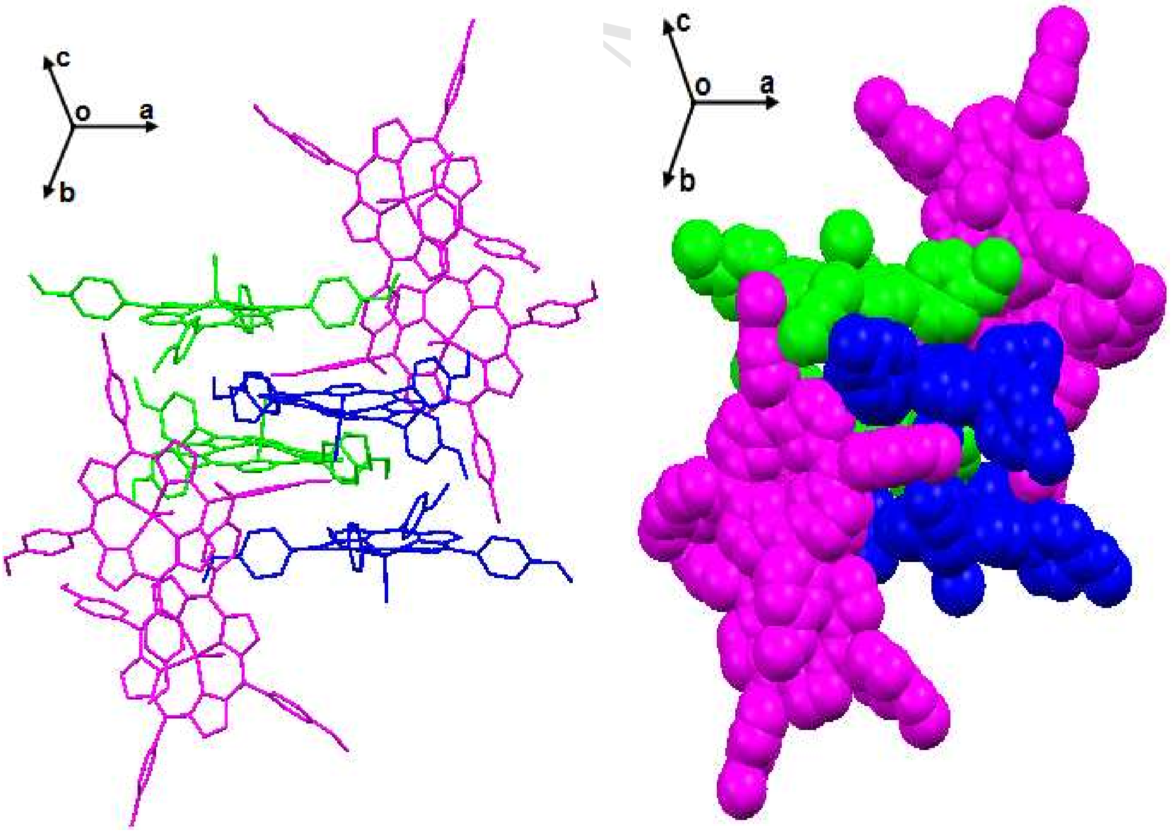

Fig. 4 Capped stick (left) and space filled (right) models in the crystal packing of **I** showing the offset or slipped face-to-face stacking arrangements of monomeric units

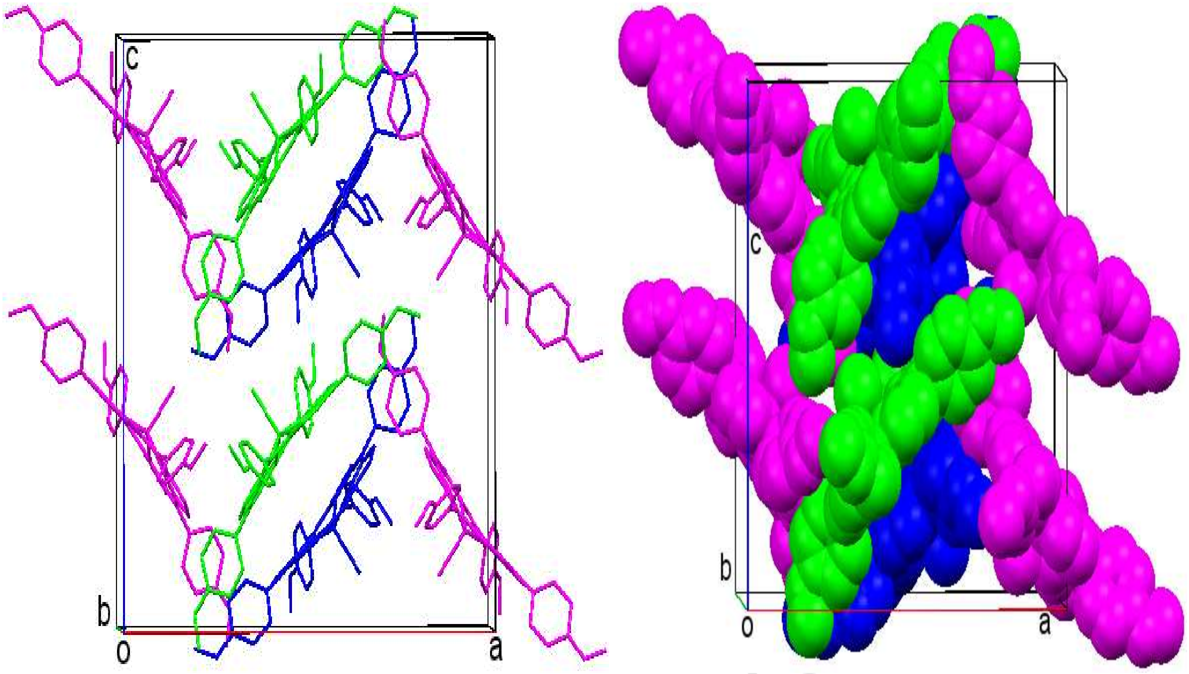

Fig. 5 Capped stick (left) and space filled (right) models in the crystal packing of **I**, showing the alignment of monomeric units as dimeric porphyrin pairs

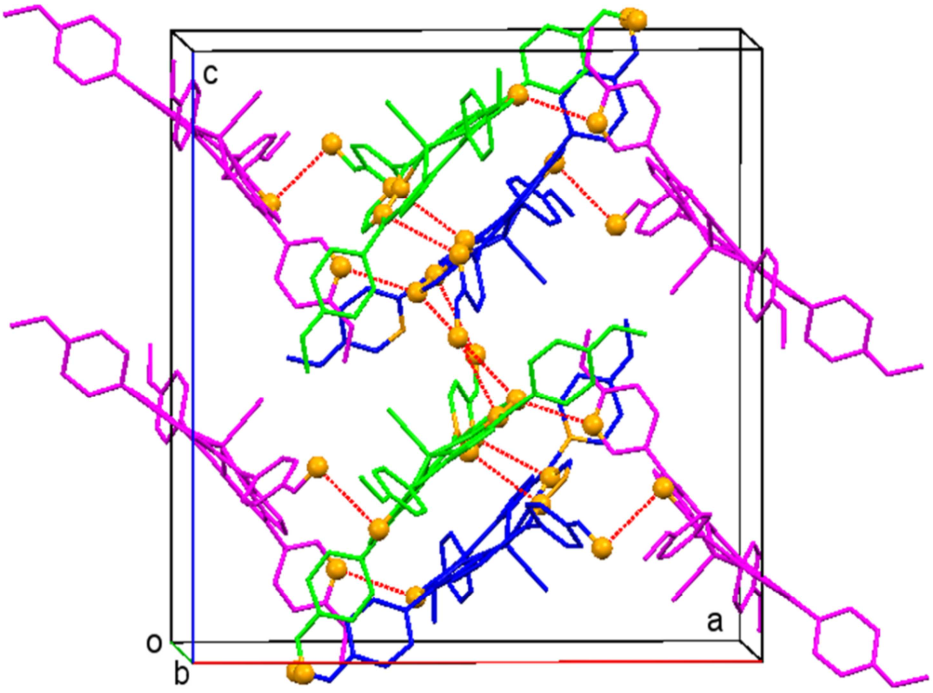

(a)

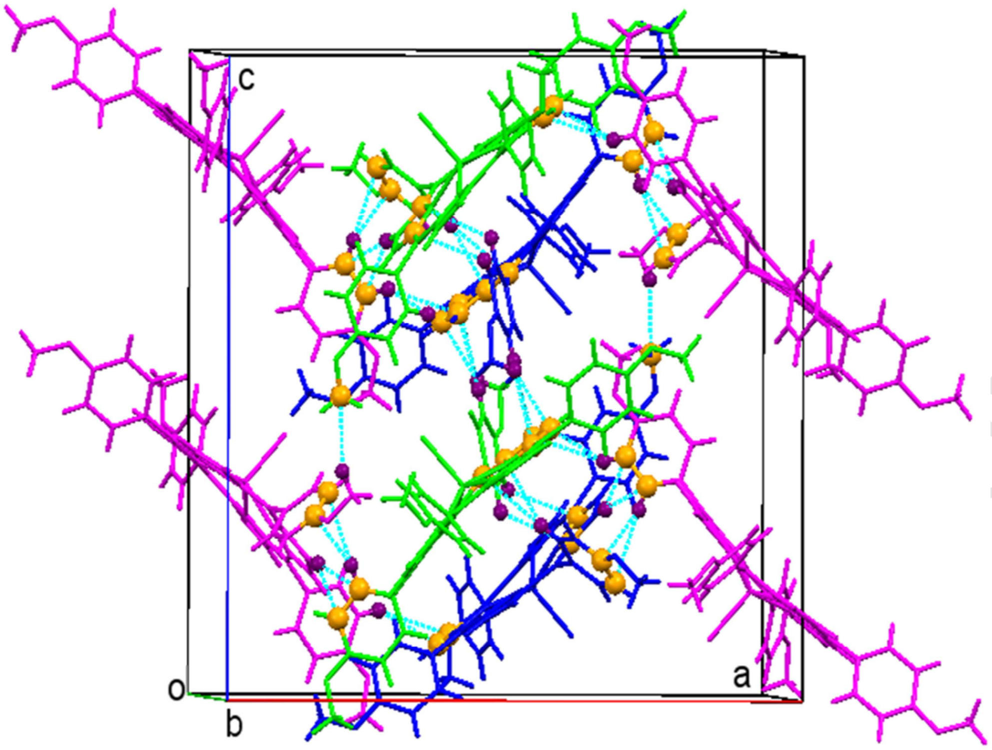

(b)

Fig. 6 Offset or slipped face-to-face stacking geometry in the crystal lattice of **I** stabilised by C···C (a) and C−H··π (b) interactions. The atoms involved in directional interactions are shown by orange (C) and purple (H) spheres

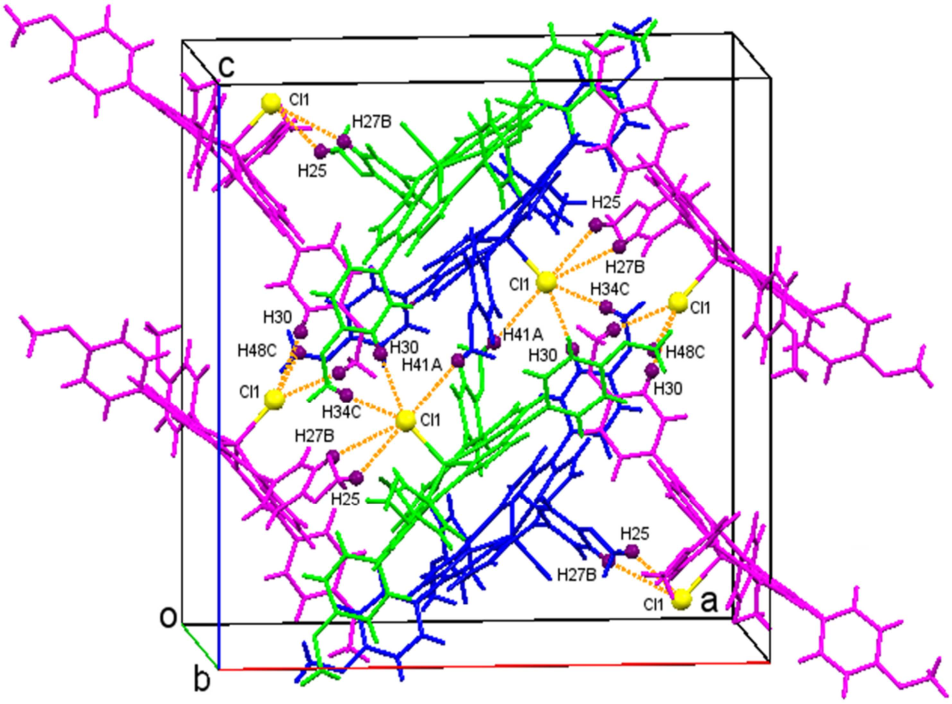

(a)

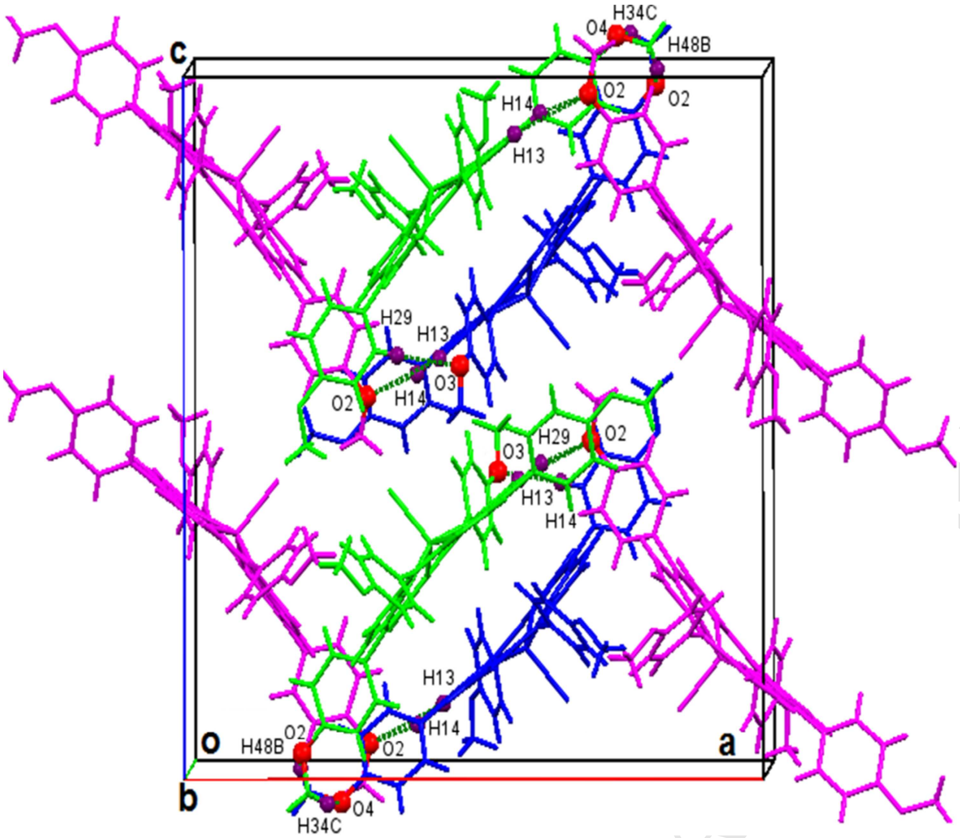

(b)

Fig. 7 Offset or slipped face-to-face stacking geometry in the crystal lattice of **I** stabilised by In−Cl···H (a) and C−O···H (b) interactions. The atoms involved in directional interactions are shown by purple (H), yellow (Cl) and red (O) spheres

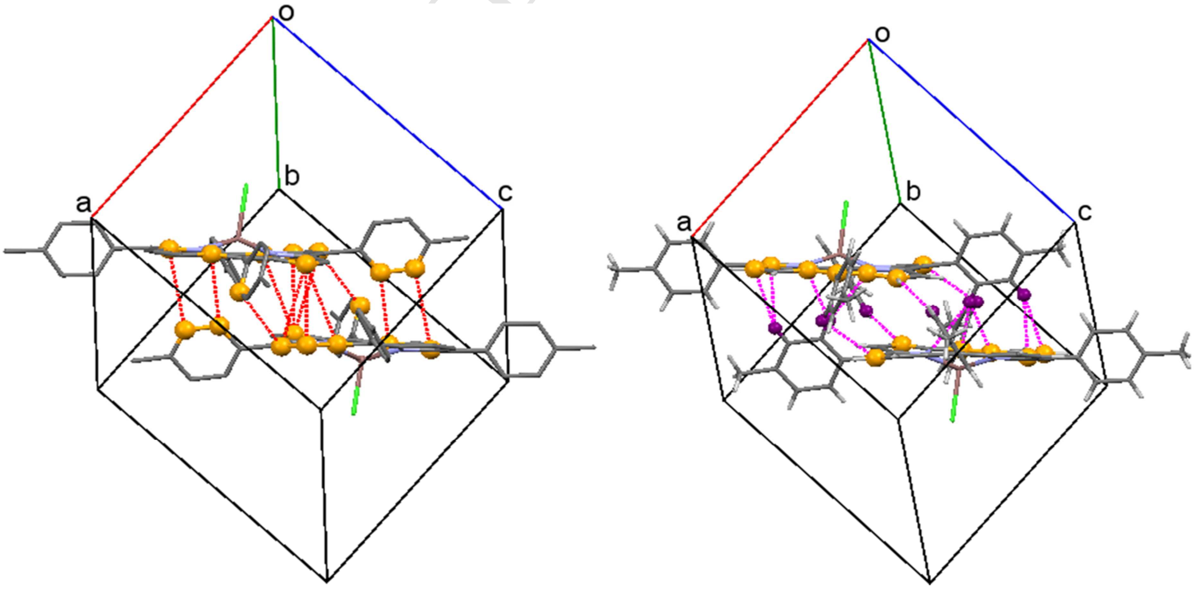

Fig. 8 Offset or slipped face-to-face stacking geometry in the crystal lattice of **II** stabilised by C···C (left) and C−H··π (right) interactions. The atoms involved in directional interactions are shown by orange(C) and purple (H) spheres

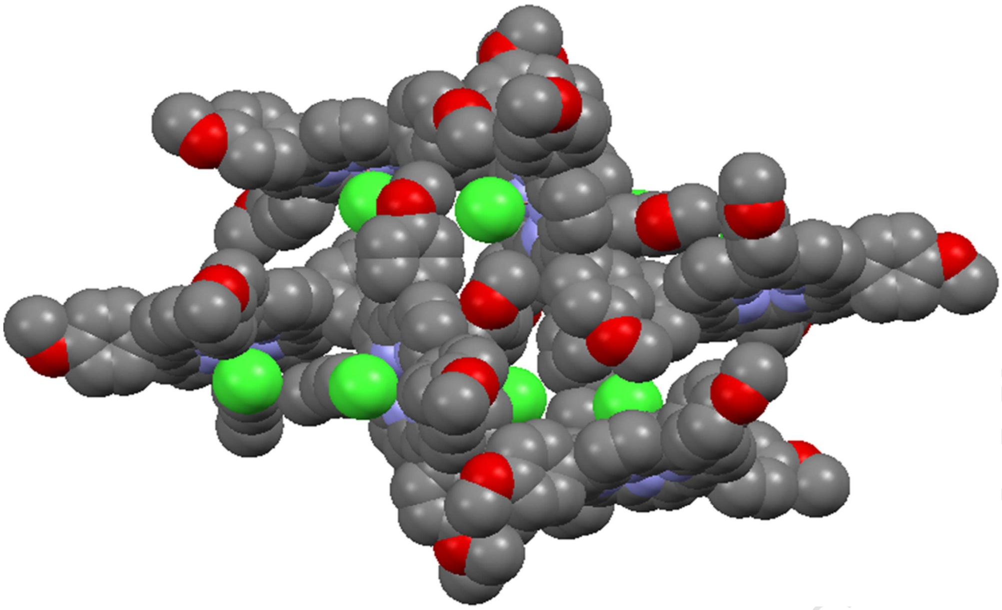

(a)

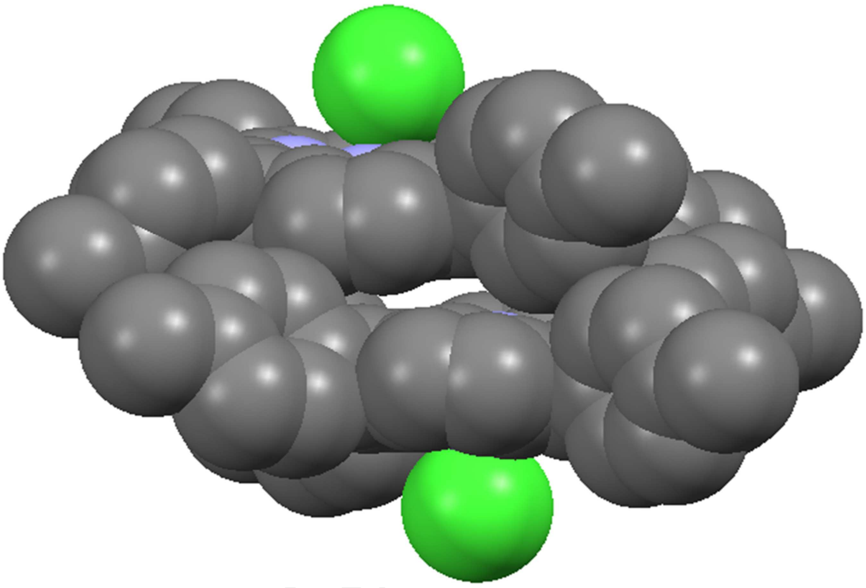

(b)

Fig. 9 Spacefilling models of **I** (a) and **II** (b) illustrating, the porosities in the crystal packings. Carbon atoms are shown in gray, oxygens in red, nitrogens in blue, and chlorine atoms in green

3.3 ^{1}H NMR spectroscopy

The selected regions of the ^{1}H NMR spectra of **I** and **II** and their corresponding free base analogues i.e. **H_2TMP** and **H_2TTP** are given in Fig. 10 and Fig. 11. ^{1}H NMR experiments were carried to better understand the influence of In^{3+} ion insertion into the porphyrinic cores of **H_2TMP** and **H_2TTP**. The displacement of In^{3+} ion above the mean porphyrinic planes as observed in the crystal structures of **I** and **II**, generates asymmetric environment above and below the plane of the macrocycles which resulted in the "magnetic inequivalence" of ortho aryl protons [9]. Hence one can easily observe two sets of doublets for ortho aryl protons (Hc) in the ^{1}H NMR spectrum of the each synthesized complex. The detection of two sets of doublets for ortho aryl protons by the pmr spectrometer becomes possible due to the slow rotation of the aryl rings about the (C−C) single bonds which connects the aryl rings to the porphyrin rings at their meso (=CH−) positions. The "magnetic inequivalence" of ortho phenyl protons was earlier arbitrarily assigned to "nonequivalence of phenyls in pairs" [1], presumably due to lack of crystal data of **I** and **II** at that time. The doublets appearing at 7.31/7.33 ppm in **I** and 7.57/7.59 ppm and 8.11/8.13 in **II** might be attributed to the presence of some unreacted free base compounds. The ^{1}H NMR spectra further demonstrates that the resonance signals corresponding to beta pyrrole protons (Ha), meta phenyl protons (Hb) and para methoxy protons (He) in case of **I** and beta pyrrole protons (Ha), meta phenyl protons (Hb) and para methyl protons (He) in **II** exhibits downfield shift, compared with the corresponding resonance signals of their free base analogues i.e. **H$_2$TMP** and **H$_2$TTP**. This indicates that the insertion of In^{3+} ion into the porphyrinic cores of **H$_2$TMP** and **H$_2$TTP** resulted in the de-protection of the phenyl as well as β-pyrrolic protons. The signals at δ -2.74 in **H$_2$TMP** and -2.76 ppm in **H$_2$TTP** are due to the resonances of the inner NH protons.

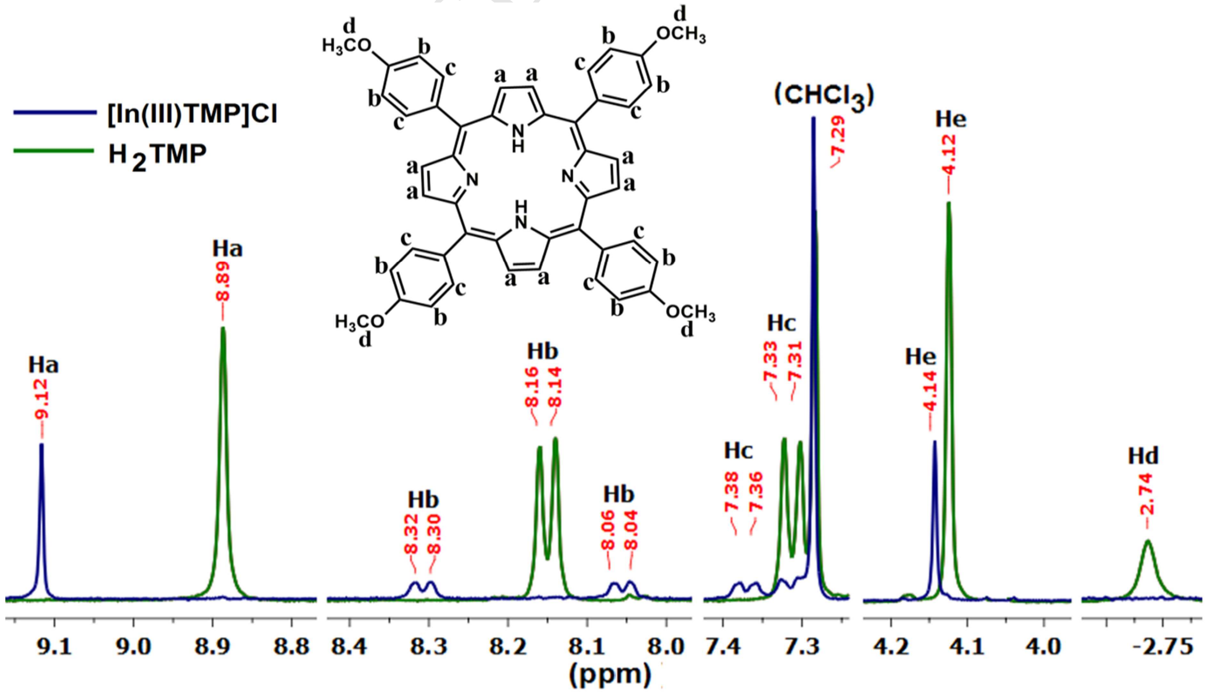

Fig. 10 The selected regions of the ^{1}H NMR spectra (400 MHz pulse FT) of **H_2TMP** (olive green,~4.0 X 10^{-5} M) and **[In(III)TMP]Cl** (blue,~5 X 10^{-3} M) in $CDCl_3$. Extra peaks at δ 7.2 ppm and 1.5-1.6 ppm are due to presence of undeuterated chloroform and water molecules

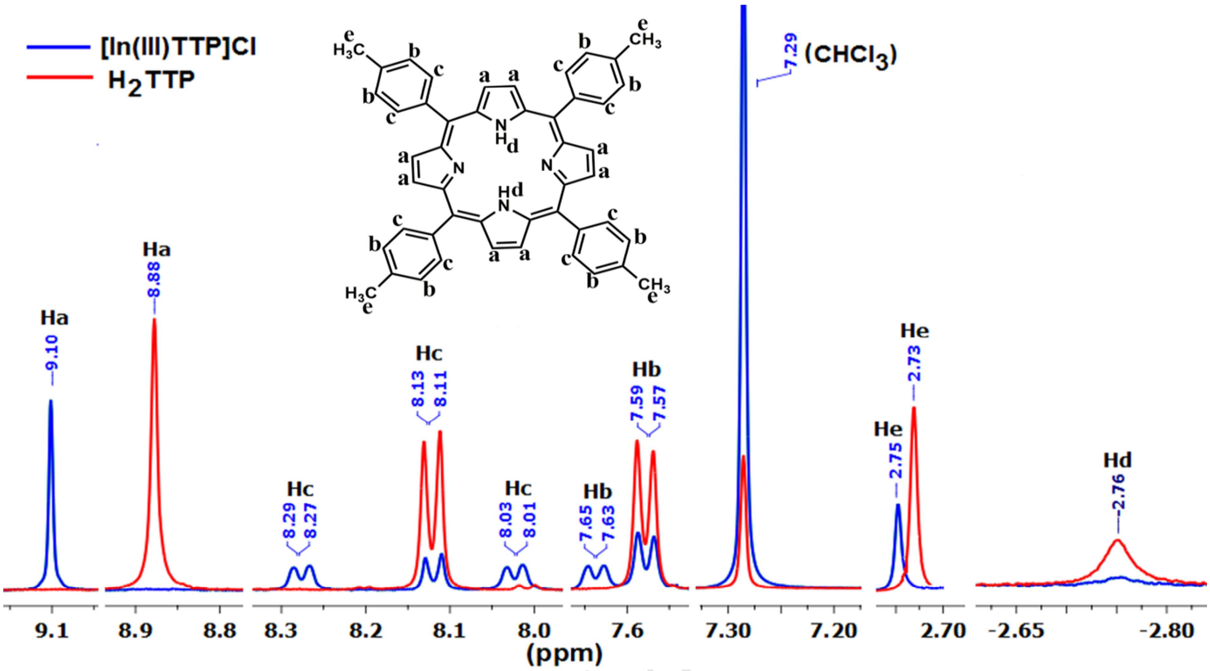

Fig. 11 The selected regions of the ^{1}HNMR spectra (400 MHz pulse FT) of **H_2TTP** (red,~4.0 X 10^{-5} M) and **[In(III)TTP]Cl** (blue,~5 X 10^{-3} M) in $CDCl_3$. Extra peaks at δ 7.2 ppm and 1.5-1.6 ppm are due to presence of undeuterated chloroform and water molecules

3.4. UV-Visible spectroscopy

The electronic absorption spectra of **H_2TMP** and **H_2TTP** are highly sensitive to processes such as protonation (pH = 4), deprotonation (pH = 10) and metallation. The subtle variations in optical absorption spectra of the synthesized porphyrins have been monitored by using UV-Vis spectroscopy.

Fig. 12 shows the optical absorption spectra of **H_2TMP** and **H_2TTP** in dichloromethane under neutral (pH = 7) and acidic (pH = 4) media. Under neutral environment (pH = 7) at ~ 4.0 x 10^{-6} M, each of the free base macrocycle [scheme 1 (a)] exhibits one higher intensity soret or B band centred around λ_{max} 400nm and four weaker Q bands lying between λ_{max} 500 to 680nm range characteristic of a regular or normal porphyrin molecules. The B and Q bands arise due to the (S_0 to S_2) and (S_0 to S_1) transitions within the highly conjugated π systems [31]. The absorption spectra of the two free bases measured under the neutral conditions at~

4.0 x 10^{-6} M corresponds to the spectra of non aggregated or monomeric porphyrin moieties, since no variations were observed upon subsequent dilutions of the solutes. At high ionic strength of the media (pH = 4), the two inner imino nitrogen atoms of the N4 cores of **H_2TMP** and **H_2TTP** undergoes protonation [32] [scheme 1 (b)]. The protonation induces partial positive charge in the centre of the molecules thereby producing dicationic type species. The dication generations led to the appearance of a narrow higher energy and red shifted band (known as J-band), followed by reduction in the number of Q bands and appearance of a single higher intensity Q band in each free base porphyrin (Fig. 12). From the literature data, it is found that J-band for **H_2TMP** appears at λ_{max} 451nm in THF-aqueous solution at pH = 4 and lower [32]. This indicates that the media in which the protonation of porphyrins occurs at low pH plays significant role in deciding the positions of absorption bands of porphyrins under aggregated conditions. The dramatic change in the spectra of **H_2TMP** and **H_2TTP** under acidic conditions (pH = 4) are attributed to the prominent self aggregation of the monomers induced by protonation of inner imino nitrogen atoms. The prominent red shift of absorption bands, especially, the B bands strongly signifinies that both the free bases undergo J-type supramolecular aggregation [33]. The decrease in the number of Q bands is attributed to increase of the D_2h symmetry of the free base porphyrins to D_4h by protonation. The symmetry group of the free-base porphyrins are D_2h due to the two hydrogen atoms located diagonally on the pyrrolic nitrogens, the porphyrins without these protons are of higher symmetry [34]. Another important phenomenon observed under acidic conditions is the appearance of charge transfer electronic bands (hyperporphyrin effects) in both the free bases. The charge transfer optical bands were found at λ_{max} 326 and 366nm for **H_2TMP** and **H_2TTP**. The charge transfer spectra arise due to transition from peripheral para substituted phenyl groups to empty π^* orbitals of porphyrins [35]. Because of the charge transfer transitions, the color of the solutions changes from purple to green. At pH = 10, the porphyrin rings of **H_2TMP** and **H_2TTP** undergoes deprotonation [36] and produces dianionic type moieties [scheme 1 (c)]. Though the pattern of absorption band spectra of an electrically neutral and dianion porphyrins remains same, the dianion generations induces profound increase in the intensities of B as well as Q bands (Fig. S1). The hyperporphyrin effects have not been observed for the two free bases under basic media (pH = 10). It can be observed from Fig. 12 that the absorption bands of **H_2TMP** are slightly red shifted in comparison with **H_2TTP**. The red shift is due to the greater electron donating tendency of the para methoxy substituents as compared to para methyl substituents resulting in the increase in π conjugation and reduction of the HOMO–LUMO energy gap [37].

The optical absorption spectra of **I** and **II** at pH = 7 at very low concentrations~4.0 x 10^{-6}M reflects that both the complexes exists as simple monomers consisting of one sharp soret band and only two Q bands characteristics of porphyrin coordinated to a metal ion through the four Nitrogen atoms. The reduction in the number of Q bands in metalloporphyrins is attributed to the increase in the symmetry (D_2h) of the free base porphyrins to D_4h by metallation [38]. The most striking feature is the absorption spectral data of the two In^{3+} complexes at high ionic strength of the media. The two metalloporphyrins exhibits completely different stability in acidic environments. The measurement of absorption spectrum of **I** in CH_2Cl_2 [Fig. 14 (left)] at pH = 5 and lower exhibits no change in the positions and number of absorption bands of the metalloporphyrin indicating remarkably high stability of the complex in media of high ionic strength. This further reflects that the protons of the acid could not replace the In^{3+} ion from the macrocyclic ring of **H_2TMP** which may be attributed to relatively strong coordination of In^{3+} to the four Nitrogen atoms of the porphyrinic core of **H_2TMP**. On the contrary, metalloporphyrin **II** exhibits extremely low stability even in slight acidic media. At pH~5, the purple colour of the dichloromethane solution of **II** changes to dark green followed by changes in the number and positions of the absorption bands. The soret band undergoes bathochromic shift and the two Q bands reduces to only one higher energy red shifted band. An additional band due to charge transfer transition is also observed at λ_{max}~369nm [Fig. 14 (right)]. This band is red shifted by λ_{max} 3nm compared with that of free base porphyrin measured under acidic media [Fig. 12 (right)]. All these spectral changes in complex **II** indicates that In^{3+} ions are being easily replaced by the protons of the acid to give the corresponding protonated free base compounds. The protonated species thus generated simultaneously undergoes J-type molecular aggregation giving one higher energy J-band and one Q band. The extremely low stability of complex **II** in acidic media may be due to weak coordination of In^{3+} ion to the four nitrogens of **H_2TTP**. The relatively strong and weak coordination of the In^{3+} ions to the nitrogen atoms of the two free bases is also reflected from the average In−N bond distance parameters which are found to be 2.146 Å [**I**] and 2.153 Å [**II**]. Although the difference in the average In−N bond distances in **I** and **II** is very low, there may be some additional factors that accounts for the different stability of the two metalloporphyrins in acidic media. The insertion of In^{3+} ions into the porphyrinic cores of **H_2TMP** and **H_2TTP** resulted in the bathochromic shift of B as well as Q bands (Fig. 14). The red shift of absorption bands in In^{3+} porphyrins (heavy metal porphyrins) can be attributed to the fact that the metal orbitals are closer in energy to the antibonding π^* molecular orbitals (lowest unoccupied molecular orbitals, LUMOs) than to the bonding, π molecular orbitals (highest occupied molecular orbital, HOMO) of porphyrin, so that the perturbation they generate reduces the energy of the LUMOs more than that of the HOMO, resulting in the bathochromic shift of π-π* transitions [39].

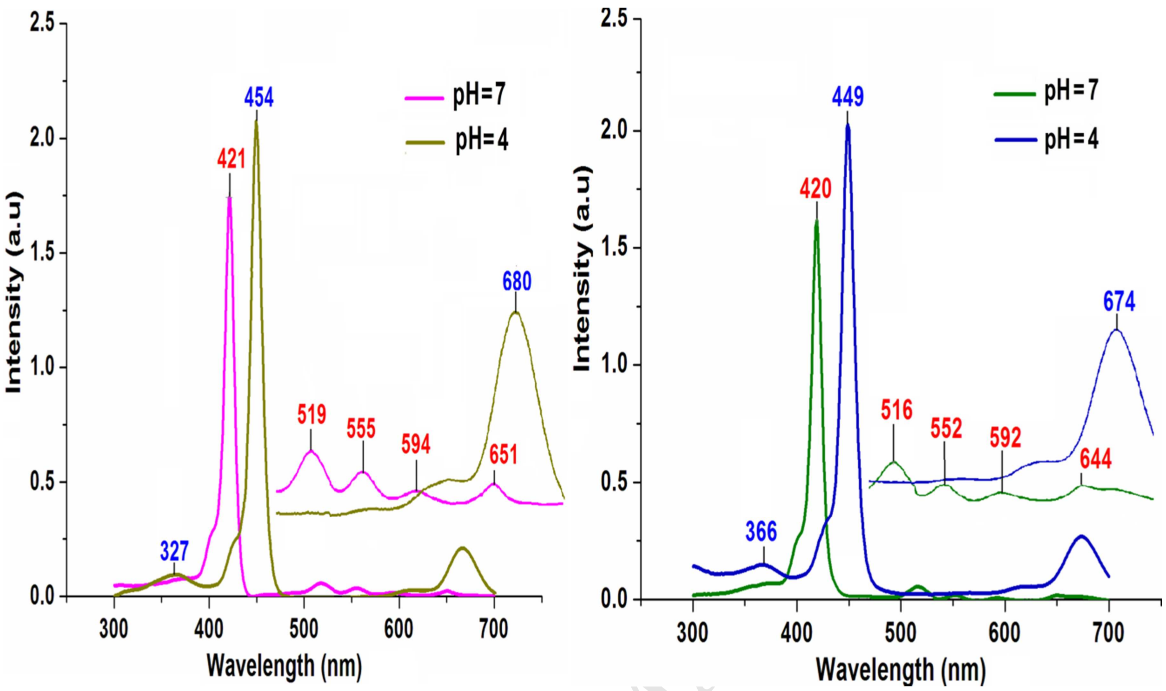

Fig. 12 The UV/Vis absorption spectra of **H_2TMP** at (a) pH = 7 (magenta) and (b) pH = 4 (green) [left] and **H_2TTP** at (a) pH = 7 (olive green) and (b) pH = 3 (blue) [right] in CH_2Cl_2

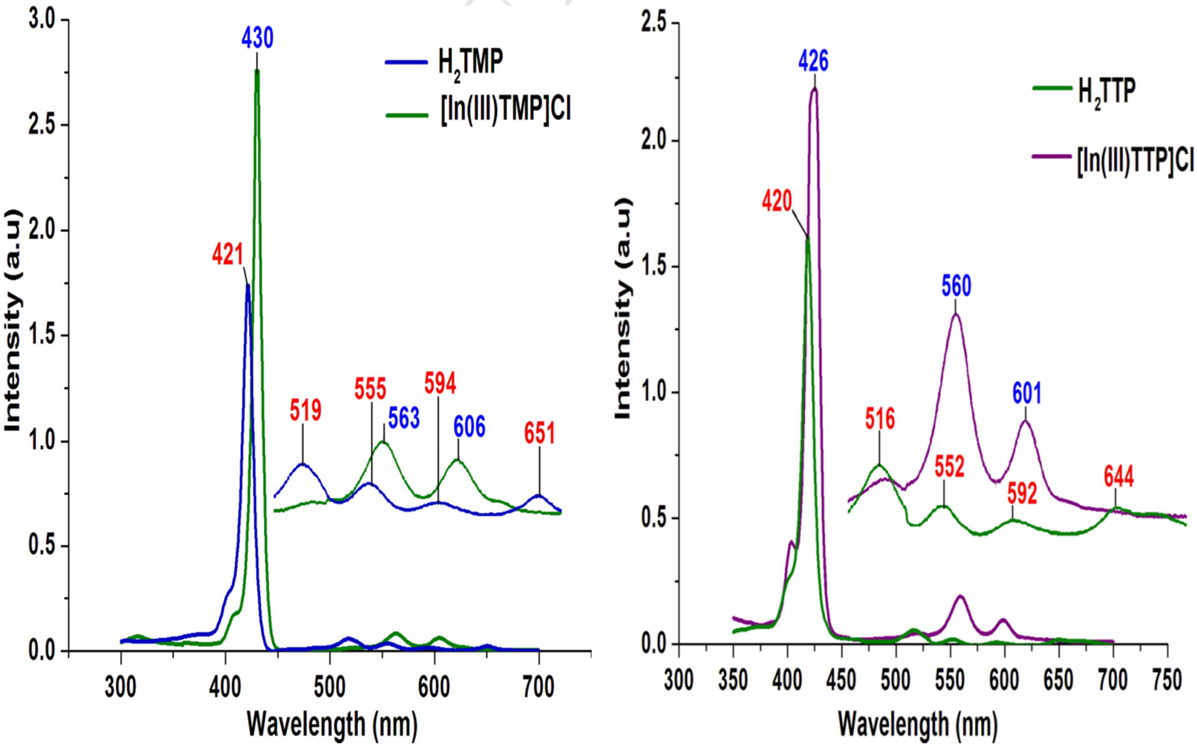

Fig. 13 The UV/Vis absorption spectra of **H_2TMP** (blue) and **[In(III)TMP]Cl** (olive green) [left] and **H_2TTP** (olive green) and **[In(III)TTP]Cl** (purple) [right] in CH_2Cl_2 at pH = 7 at ~ 4.0 x 10^{-6}M

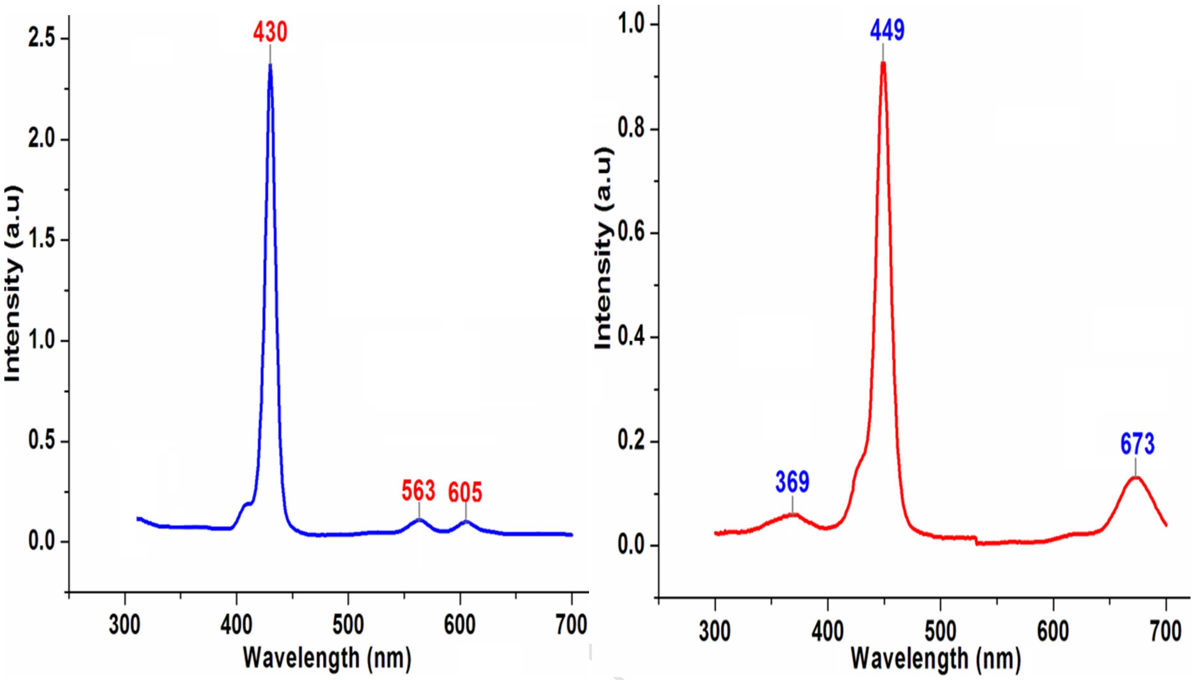

Fig. 14 The UV/Vis absorption spectra of **[In(III)TMP]Cl** [left] and **[In(III)TTP]Cl** [right] in CH_2Cl_2 at pH = 5 and lower at ~4.0 x 10^{-6}M

4. Conclusions

In summary we have reported the single crystal molecular structures of **I** and **II**. Both the macrocycles have "dome shaped" structures due to the pulling of In^{3+} ions above the mean planes of four nitrogen atoms. Further the two metal complexes exhibit J-type stacking of their monomeric rings. From the absorption measurement data, it is confirmed that both **H_2TMP** and **H_2TTP** exist as distinct monomers in neutral media at lower molar concentrations~4.0 x 10^{-6}M. However, under high ionic strength of the media, they tend to aggregate in J-type molecular alignments. Also under such media both the metal free compounds undergoes charge transfer transitions characteristics of a hyper porphyrin dye materials. A tremendous increase in the intensities of the absorption bands of **H_2TMP** and **H_2TTP** is observed under the basic media. The two metal complexes exist as simple monomers in neutral media at lower molar concentrations~4.0 x 10^{-6}M. In media of high ionic strength (pH = 5 and lower), the In^{3+} ion in metalloporphyrin **I** remain intact with the macrocyclic ring thereby reflecting high stability of the complex. However in **II**, In^{3+} ion is easily demetallated from the macro ring to give the protonated free base species which undergoes simultaneous J-type aggregation. The insertion of In^{3+} ions within the porphyrinic cores of H_2TMP and H_2TTP induces bathochromic shifts and increase in the intensities of the absorption bands. In the end, the displacement of In^{3+} ion above the mean porphyrin plane in each complex result in the “magnetic inequivalence” of ortho phenyl protons.

Acknowledgments

This research was supported by Council of Scientific and Industrial Research (CSIR) India (grant No. 09/100(0190)/2016-EMR-I).

References

1. M. Ethirajan, Y. Chen, P. Joshi, R. K. Pandey, Chem. Soc. Rev., 40 (2011) 340-362.

2. A. J. Mozer, M. J. Griffith, G. Tsekouras, P. Wagner, G. G. Wallace, S. Mori, K. Sunahara, M. Miyashita, J. C. Earles, K. C. Gordon, L. Du, R. Katoh, A. Furube, D. L. Officer, J. Am. Chem. Soc., 131 (2009) 15621-15623.

3. M. J. Griffith, K. Sunahara, P. Wagner, K. Wagner, G. G. Wallace, D. L. Officer, A. Furube, R. Katoh, S. Mori, A. J. Mozer, Chem. Commun., 48 (2012) 4145–4162.

4. Y. Nakamura, N. Aratani, A. Osuka, Chem. Soc. Rev., 36 (2007) 831–845.

5. A. V. Teles, T. M. A. Oliveira, F. C. Bezerra, L. Alonso, A. Alonso, I. E. Borissevitch, P. J. Goncalves, G. R. L. Souza, J Gen Virol., 99 (2018) 1301-1306.

6. T. Lee, X. Zhang, S. Dhar, H. Faas, S. J. Lippard, A. Jasanoff, Chem. Biol., 17 (2010) 665–673.

7. A. R. Silva, A. C. Pelegrino, A. C. Tedesco, R. A. Jorge, J. Braz. Chem. Soc., 19 (2008) 491-501.

8. M. Bhatti, W. Bhatti, E. Mast, J. Inorg. Nucl. Chem., 8 (1972) 133-137.

9. R. G. Ball, K. M. Lee, A. G. Marshall, J. Trotter, Inorg. Chem., 19 (1980) 1463-1469.

10. T. N. Hong, Y. H. Sheu, K. W. Jang, J. H. Chen, S. S. Wang, J. C. Wang, S. L. Wang, Polyhedron, 15 (1996) 2647-2654.

11. Y. Yi Lee, J. H. Chen, H. Y. Hsieh, Polyhedron, 22 (2003) 1633-1639.

12. C. H. B. Cloutour, L. Mauclaire, M. Pereyre, S. Adams, M. Drager, Polyhedron, 9 (1990) 1297-1303.

13. P. G. Parzuchowski, J. W. Kampf, E. Rozniecka, Y. Kondratenko, E. Malinowska, M. E. Meyerhoff, Inorganica Chimica Acta., 355 (2003) 302-313.

14. R. Guilard, P. Cocolios, P. Fournari, J. Organomet. Chem., 129 (1977) C11-C13.

15. S. M. Andrade, R. Teixeira, S. M. B. Costa, A. J. F. N. Sobral, Biophys. Chem., 133 (2008) 1-10.

16. R. K. Pandey, U. Chitgupi, V. Lakshminarayanan, J. Porphyr.Phthalocyanines 16 (2012) 1055-1058.

17. M. Shirakawa, K. Nakata, M. Suzuki, T. Kobayashi, E. Tokunaga, J. Phys. Soc. Jpn., 86 (2017) 1-7.

18. N. K. Giri, A. Banerjee, R. W. J. Scott, M. F. Paige, R. P. Steer, Phys. Chem. Chem. Phys., 16 (2014) 26252-26260.

19. F. C. Spano, S. Mukamel, Phys. Rev. A, 40 (1989), 5783-5801.

20. P. W. Bohn, Annu. Rev. Phys. Chem., 44 (1993), 37-60.

21. V. Czikklely, H. D. Forsterling, H. Kuhn, Chem. Phys. Lett., 6 (1970), 207-210.

22. F. Nuesch and M. Gratzel, Chem. Phys., 1995, 193, 1-17.

23. O.V. Dolomanov, L.J. Bourhis, R. J. Gildea, J.A.K. Howard, H. Puschmann, J. Appl. Cryst., 42 (2009) 339-341.

24. G.M. Sheldrick, Acta Cryst., A64 (2008) 112-122.
25. A. D. Adler, F. R. Longo, J. D. Finarelli, J. Goldmacher, J. Assour, L. Korsakoff, J. Org. Chem., 32 (1967) 476.

26. N. C. Maiti, M. Ravikanth, S. Mazumdar, N. Periasamy, J. Phys. Chem., 99 (1995) 17192-17197.
27. N. C. Maiti, S. Mazumdar, N. Periasamy, Curr. Sci., 70 (1996) 997-999.
28. N. C. Maiti, S. Mazumdar, N. Periasamy, J. Phys. Chem. B, 102 (1998) 1528-1538.

29. C. A. Hunter, J. K. M. Sanders, J. Am. Chem. Soc., 112 (1990) 5525–5534.
30. C. R. Martinez, B. L. Iverson, Chem. Sci., 3 (2012) 2191-2201.
31. W. Zheng, N. Shan, L. Yu, X. Wang, Dyes and Pigments 77 (2008) 153-157.
32. E. Fagadar-Cosma, C. Enache, R. Tudose, I. Armeanu, E. Mosoarca, D. Vlascici, O. Costisor. Rev. Chim. (Bucuresti)., 58 (2007) 451-455.
33. F. Wurthner, T. E. Kaiser, C. R. Saha-Moller, Angew. Chem. Int. Ed., 50 (2011) 3376-3410.
34. P. J. Spellane, M. Gouterman, A. Antipas, S. Kim, Y. C. Liu, Inorg. Chem., 19 (1980) 386-391.
35. J. R. Weinkauf, S. W. Cooper, A. Schweiger, C. C. Wamser, J. Phys. Chem. A, 107 (2003) 3486-3496.
36. H. Guo, J. Jiang, Y. Shi, Y. Wang, Y. Wang, S. Dong, J. Phys. Chem. B, 110 (2006) 587-594.
37. J. Dalton, L. R. Milgrom, S. M. Pemberton, J. Chem. Soc., Perkins 2, 0 (1980) 370-372.
38. S. Ishihara, J. Labuta, W. V. Rossom, D. Ishikawa, K. Minami, J. P. Hill, K. Ariga, Phys. Chem. Chem. Phys., 16 (2014) 9713-9746.
39. G. D. Bajju, Deepmala, V. Kumar, S. Kundan, A. Ahmed, WJPR, 3 (2014) 1613-1622.

- Insertion of In^{3+} ions within the porphyrin cores of H_2TMP and H_2TTP causes dome-type structures of the macrocyclic rings.
- Absorption bands in two In^{3+} porphyrins are bathochromically shifted as compared to their free base analogs.
- In basic media, the two In^{3+} porphyrins exhibit significant increase of their absorption band intensities.
- The In^{3+} derivative of H_2TMP is fairly stable under acidic environment. However, the In^{3+} ion is easily released from the porphyrin core of H_2TTP under such media.